ACS OMEGA

Open Access

http://pubs.acs.org/journal/acsodf

Article

Meshed, Flexible, and Self-Supported Humidity Sensors by Direct-Writing with Multifunctional Applications

Chengli Tang,* Haoxiang Wang, Yuhao Dou, and Puguo Lai

Cite This: *ACS Omega* 2024, 9, 33261−33269

Read Online

ACCESS | Metrics & More | Article Recommendations | Supporting Information

ABSTRACT: Flexibility endows humidity sensors with new applications in human health monitoring except for traditionally known environmental humidity detection in recent years. In this study, a flexible, mesh-structured, and self-supported humidity sensor was designed and manufactured by direct writing in a homemade two-dimensional stepping numerical control workstation. Bacterial cellulose with humidity sensitivity and good film-forming properties was applied as the self-supporting substrate, in which conductive activated carbon and water-absorptive magnesium chloride ($MgCl_2$) were incorporated. The humidity sensing performance of the printed sensor was measured and optimized. Besides, the fundamental insight into the sensing mechanism of the printed humidity sensor was analyzed by a complex impedance spectrum. The multifunctional applications of the self-supported humidity sensor were demonstrated by human breathing detection, noncontact distance sensing, and speaking recognition. The simple self-supported structure combined with the meshed attribute of the flexible sensor showed large use potential in real-time monitoring of human respiration, voice detection, environmental humidity monitoring, and noncontact switches.

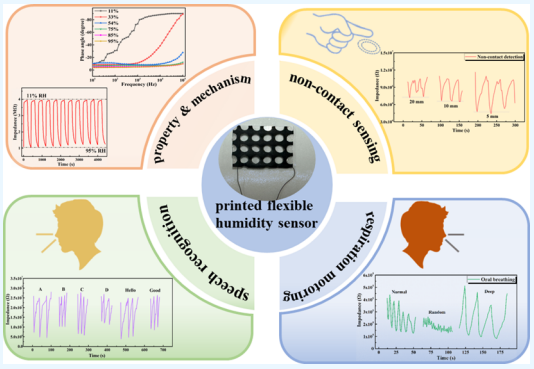

INTRODUCTION

Humidity, or relative humidity (RH), is an environmental factor that plays a crucial role in industrial, agricultural production, and medical practice.[1−5] Various humidity sensors are in essential need for these scenarios, where RH needs accurate monitoring, regulation, and control. With the advancements in wearable devices and flexible electronics, a diverse range of flexible humidity sensors, including resistive, impedance, capacitive, and even self-powered types, have been reported for accurate humidity detection.[6−8] The flexibility attribute of humidity sensors endows them with new applications like human health-related monitoring, noncontact switches, etc.[9−13] For example, a flexible humidity sensor was used for monitoring human respiration to identify different breathing statuses and behaviors.[8,11,12] Since abnormal respiratory frequency and intensity are telltale symptoms of respiratory diseases. The detection of human respiration can offer valuable assistance in diagnosing sleep apnea syndrome, asthma, cardiac arrest, and cardiovascular and cerebrovascular diseases. Real-time or continuous and precise monitoring of respiration allows for earlier detection of abnormalities, which is of immense significance for early disease detection and effective treatment to provide robust health safeguards for patients.[14,15] Besides, humidity sensor-based noncontact switch can be used in the human-machine interaction to replace the traditionally applied contact hardware such as computer keyboards, mouses, touch screens, etc.[16] The noncontact human-machine interaction can lower the risks of viruses/bacteria spread.

Resistance or impedance-type chemical sensors with simple structures have been greatly developed as a promising sensing device to achieve various applications including health monitoring.[17−25] There are three-layered structured humidity sensors including substrate, electrode, and sensing film. For example, Wu et al.[17] fabricated a resistive humidity sensor on a flexible liquid crystal polymer substrate, on which carbon nanocoils bridged the gaps on the Au interdigital electrodes. Molybdenum disulfide (MoS_2) ink was aerosol-jet printed on a PET substrate containing Au/Cr interdigital electrodes to prepare a humidity sensor by Pereira et al.[18] Further simplification of sensor structures was realized by integrating the electrode with a sensing layer, or substrate with a sensing layer, or the substrate with an electrode. For example, Zhu et al.[19] reported a paper-based flexible humidity sensor. It consisted of a rationally designed bilayered structure consisting of a nanoporous cellulose nanofiber/carbon nanotube sensitive layer and a microporous paper substrate. Li et al.[20] fabricated a

Received: June 5, 2024
Revised: July 9, 2024
Accepted: July 12, 2024
Published: July 18, 2024

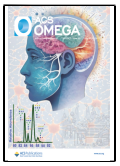

flexible and breathable humidity sensor for skin humidity monitoring. The sensor includes shape memory poly(lactic acid) fiber as the substrate and crumpled graphene oxide membrane as the top humidity-sensitive layer. Guan et al.[21] fabricated self-supported polymer films by the thiol-ene click cross-linking reaction, on which the interdigitated electrodes were screen printed with silver paste to obtain a humidity sensor. The self-supported film acts as both the sensor substrate and the humidity-sensing material. Pan et al.[22] fabricated a carbon nanotube/carbon nanofiber (CNT/CNF) composite flexible humidity sensor via near-field electrohydrodynamic direct writing. The thin CNT/CNF sensing film on a flexible poly(ethylene terephthalate) substrate was designed in the form of a quadrilateral grid to facilitate the full absorption of moisture by the CNTs. Our previous work reported on cellulose and conductive tape-based flexible humidity sensors, which combined the flexible substrate and electrode within the conductive tape.[23]

The simplest structured humidity sensor is undoubtedly one layer that simultaneously acts as the substrate, electrode, and sensing film. Zhu et al.[26] reported a flexible cellulose nanofiber/carbon nanotube (NFC/CNT) humidity sensor with high sensitivity performance developed via fast vacuum filtration. A transparent and flexible cellulose/KOH composite ionic film was fabricated as a humidity sensor via a simple casting method by Wang et al.[27] Guan et al.[28] fabricated a glycidyl trimethylammonium chloride (EPTAC) modified cellulose paper humidity sensor via a facile solution method. The paper was used for the purpose of the humidity sensing material and the sensor substrate. Zhu et al.[29] demonstrated the direct CO_2-laser writing of electrodes onto 2,2,6,6-tetramethylpiperidine-1-oxyl radical (TEMPO)-oxidized cellulose paper to realize an all-cellulose-derived humidity sensor.

With the advent of the wearable smart device society, there is a growing requirement for miniaturization and conformability of the humidity sensor. When used for real-time or wearable human health detection, the humidity sensor should be miniaturized, portable, comfortable, and skin-friendly. Breathable humidity sensors are more attractive than those that are made of airtight-based materials[30−32] from this aspect. Ryotaro et al.[33] employed nanomesh electrodes to create a humidity sensor for monitoring skin epidermis humidity. These electrodes, with their biocompatible properties, adhere seamlessly to the skin surface without hindering the evaporation of water from the skin. They also exhibit a certain degree of air permeability. However, the flexibility of the sensor needs further improvement to guarantee enough comfort for the user. Furthermore, a simple and cost-effective preparation method is also in demand for facile and rapid fabrication of humidity sensors instead of complex manufacturing processes.

In this study, a flexible humidity sensor with a meshed structure was directly printed via a homemade two-dimensional stepping numerical control workstation. A composite material consisting of bacterial cellulose (BC), activated carbon (AC), and $MgCl_2$ was printed onto the surface of polyimide (PI). After drying, the printed film was completely detached from the PI surface to form a self-supported humidity sensor. It is more integrated by combining the sensing film with the supporting substrate in the self-supporting humidity sensor. The designed circular mesh-structured pattern endows the sensor with outstanding breathability. Detailed characterizations in morphological and compositional information on the sensor were conducted. The humidity sensing performance of the sensor was tested, and the sensing mechanism was explored. The potential multifunctional applications of the prepared humidity sensor in respiratory monitoring, noncontact switches, and voice detection were also demonstrated.

EXPERIMENTAL SECTION

Materials. The bacterial cellulose dispersion (BC 2s dispersion) with a solid content of approximately 0.8%, diameter ranging from 50 to 100 nm, and length exceeding 20 μm was purchased from Guilin Qihong Technology Co., Ltd. $MgCl_2{\cdot}6H_2O$ was obtained from Shanghai Sinopharm Chemical Reagent Co., Ltd. The activated carbon with a specific surface area (SSA) of 1800 m^2/g was purchased from Jiangsu Xianfeng Nanomaterials Technology Co., Ltd. All materials mentioned above were used directly without further purification or processing.

Preparation of BC/AC/$MgCl_2$ Composite Material. Activated carbon powder was dispersed in the bacterial cellulose dispersion with ultrasonic treatment for 30 min, followed by magnetic stirring for 2 h to achieve a uniform mixture. Composite solutions with concentrations of 0.1, 0.2, 0.3, and 0.4 wt % of AC were obtained by varying the mass percentage. The hygroscopic metal salt of $MgCl_2$ (with mass percentages of 0.5, 1, and 2 wt %) was further added and mixed through magnetic stirring for 1 h for the preparation of the BC/AC/$MgCl_2$ composite containing different contents of AC and $MgCl_2$.

Fabrication of Mesh-Based Flexible Humidity Sensor. The mesh structured pattern was designed by G-coding and directly printed by a homemade two-dimensional stepping numerical control workstation as depicted in Figure 1a. The

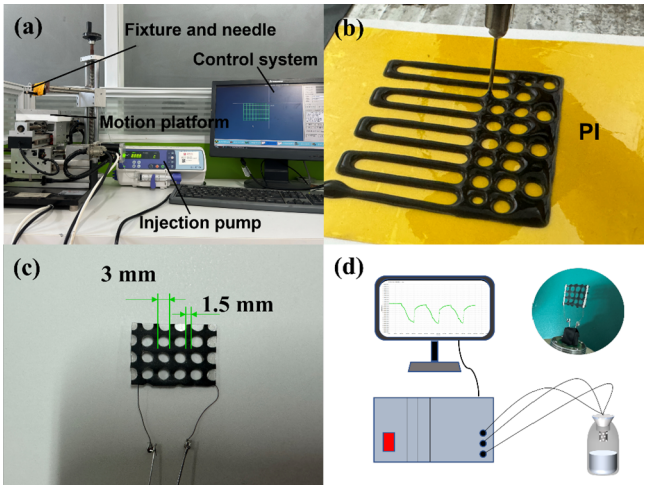

Figure 1. Photographs of (a) homemade printing equipment, (b) printing process, and (c) printed humidity sensor. (d) Electrochemical workstation for the humidity sensing test.

equipment comprises a two-axis motion platform, needle fixture, injection system (syringe pump), and control system. In the printing process, a micrometer-scale jet of the printing solution was delivered from the needle to the surface of the flexible PI substrate fixed on the motion platform. The pattern and thickness of the printed film were precisely adjustable by controlling the injection speed of the syringe pump and the motion speed of the two axes. The extrusion speed of the composite ink was set as 6 mL/h in the printing process, as

https://doi.org/10.1021/acsomega.4c05316
ACS Omega 2024, 9, 33261−33269

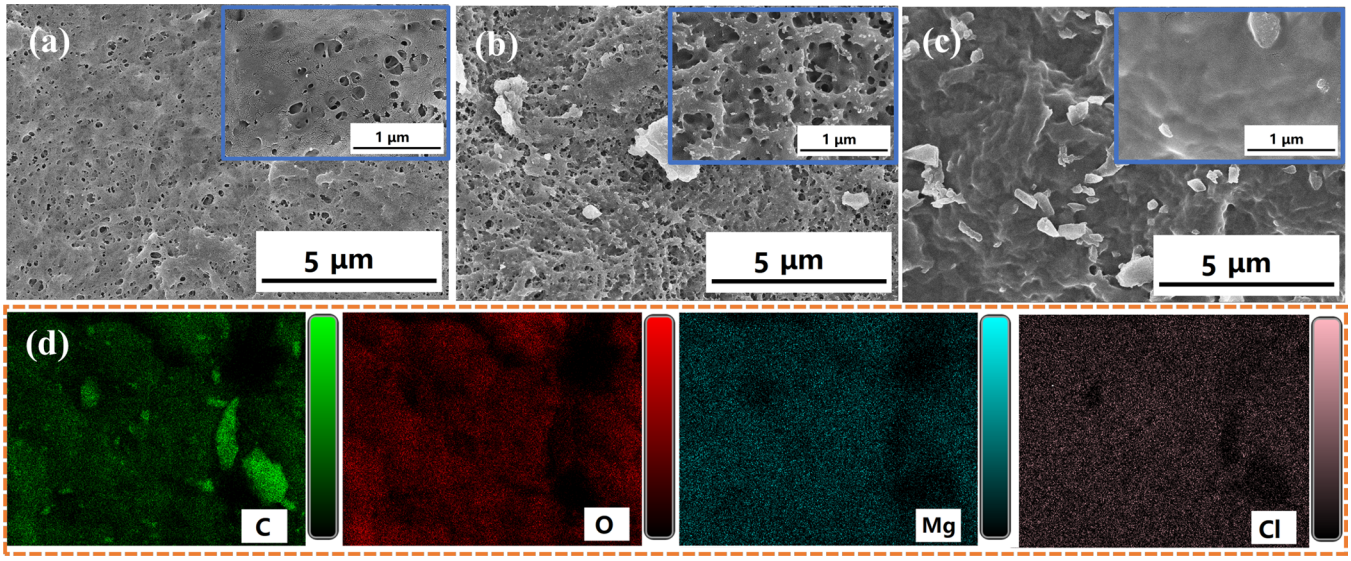

Figure 2. SEM images of (a) pure bacterial nanocellulose, (b) composite film with 0.2 wt % AC, (c) composite film with 0.2 wt % AC and 0.5 wt % $MgCl_2$, (d) elemental mapping results of C, O, Mg, and Cl in composite sensing film (content of 0.2 wt % AC and 0.5 wt % $MgCl_2$).

shown in the photo in Figure 1b. After printing and drying naturally, the circular mesh-based flexible film was removed from the PI surface. The mesh is cut into a regular rectangle and its two sides are connected with copper wire (cured by conductive silver paste) as electrodes for the following humidity-sensing performance tests. As shown in Figure 1c, the pores on the mesh pattern have a diameter of approximately 3 mm, and the distance is about 1.5 mm between each pore.

Instrumentation and Analysis. The micromorphology and surface elements of the BC/AC/$MgCl_2$ composite sensing material were characterized on a field emission scanning electron microscope (SEM, Helios 5CX, Thermo Fisher Scientific, USA) equipped with an energy dispersive spectrometer. The crystalline structure of the sensing material was analyzed using an X-ray diffractometer (XRD, Haoyuan DX 2700-BH, China). The surface hydrophilicity of the sensing film was evaluated by contact angle measured on a drop shape analyzer (DSA30S, KRUSS, Germany).

Humidity Sensitivity Tests. The humidity sensing performance of the prepared sensor was conducted in an electrochemical workstation (SA5101, Sino Aggtech), as illustrated in Figure 1d. Different saturated solutions were used to generate various RH conditions, which are also known as static humidity. Specifically, RHs of 11, 33, 54, 75, 85, and 95% were obtained by oversaturated solution of lithium chloride, magnesium chloride, magnesium nitrate, sodium chloride, potassium chloride, and potassium nitrate, respectively. The sensitivity of the sensor was evaluated by recording the impedance changes under different RHs at a frequency of 100 Hz. Additionally, complex impedance spectroscopy was conducted at various RHs to get insight into the sensing mechanism of the sensing layer with the frequency range of 10 Hz to 100 kHz.

Application Demonstration of the Humidity Sensor. In the respiratory monitoring performance test, the flexible humidity sensor was placed 3 cm in front of the mouth or nose to simulate different respiratory states. For the speaking test, the prepared humidity sensor was positioned 3 cm in front of the mouth of the volunteer to measure the humidity variations around the sensor during the pronunciation of different words. In the noncontact distance detection experiment, a finger was placed 5, 10, and 20 mm above the sensor. The impedance changes in these tests were all recorded by an SA5101 electrochemical workstation.

RESULTS AND DISCUSSION

Morphology and Composition of the Sensitive Layer. The surface morphology and elemental information on the sensitive film were analyzed by SEM observation and EDS results. The low magnification SEM image of the pure BC film in Figure S1a presents a flat surface, while a multilayered structure with numerous pores distributed across it is seen in Figure 2a. It is the typical morphology of randomly accumulated nanofibers. It increased in surface roughness when 0.2 and 0.4 wt % of activated carbon were added into the BC solution as shown in Figure S1b,c. The higher magnified image in Figure 2b for the 0.2 wt % addition of AC film remained the porous structure with carbon particles scattered on it. When 0.5 and 1 wt % of hygroscopic $MgCl_2$ were further added into the composite film, there was no obvious change in surface morphology as the low magnified SEM images (Figure S1d,e) as compared to that of the BC/AC film. However, it shows a denser surface in the higher magnified image, as shown in Figure 2c. The nanofibers are encapsulated and the pores between the fibers disappear, while the surface is still uneven. The strong hygroscopicity of $MgCl_2 \cdot 6H_2O$ allows the BC/AC/$MgCl_2$ composite film to adsorb moisture more easily, resulting in the swelling of the BC nanofiber to fill the pores between fibers and encapsulate some of the AC particles. The composite film maintained high hygroscopicity even with a denser surface structure because of the $MgCl_2$. When the mass percentage of $MgCl_2$ increased to 1 wt %, the water absorption properties of the composite film surface were further enhanced. As shown in Figure S2, the pores and activated carbon particles are almost completely covered and the surface becomes smooth and flat. Detailed surface elemental information on the composite film with a 0.2 wt % AC content and a 0.5 wt % $MgCl_2 \cdot 6H_2O$ content was conducted using energy-dispersive X-ray spectroscopy (EDS). As shown in Figures 2d and 3a,

https://doi.org/10.1021/acsomega.4c05316
ACS Omega 2024, 9, 33261−33269

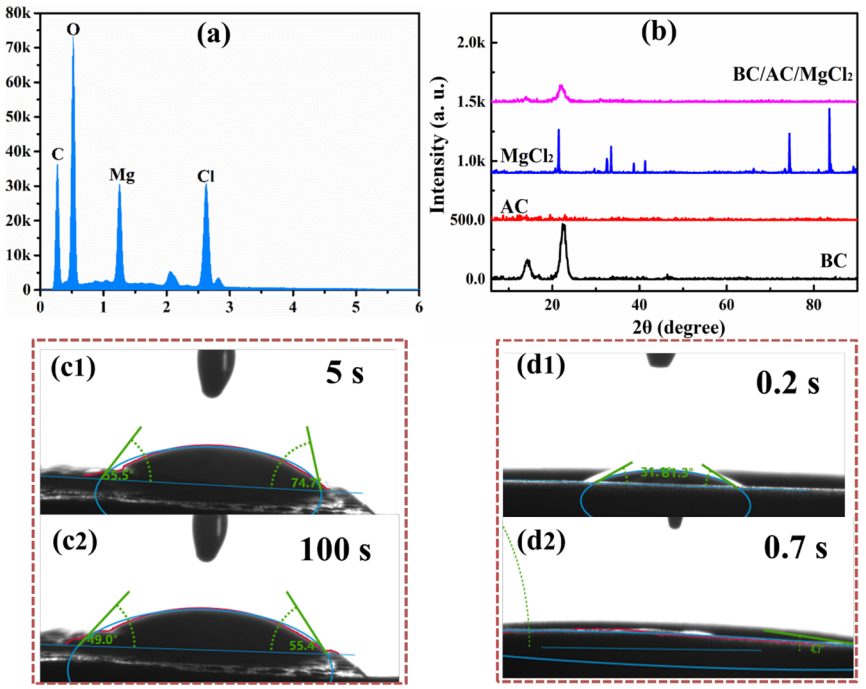

Figure 3. (a) EDS spectra of the BC/AC/$MgCl_2$ sensing film. (b) XRD pattern of the BC/AC/$MgCl_2$ sensing film. (c) Contact angle of pure BC film. (d) Contact angle of the BC/AC/$MgCl_2$ sensing film (content of 0.2 wt % AC and 0.5 wt % $MgCl_2$).

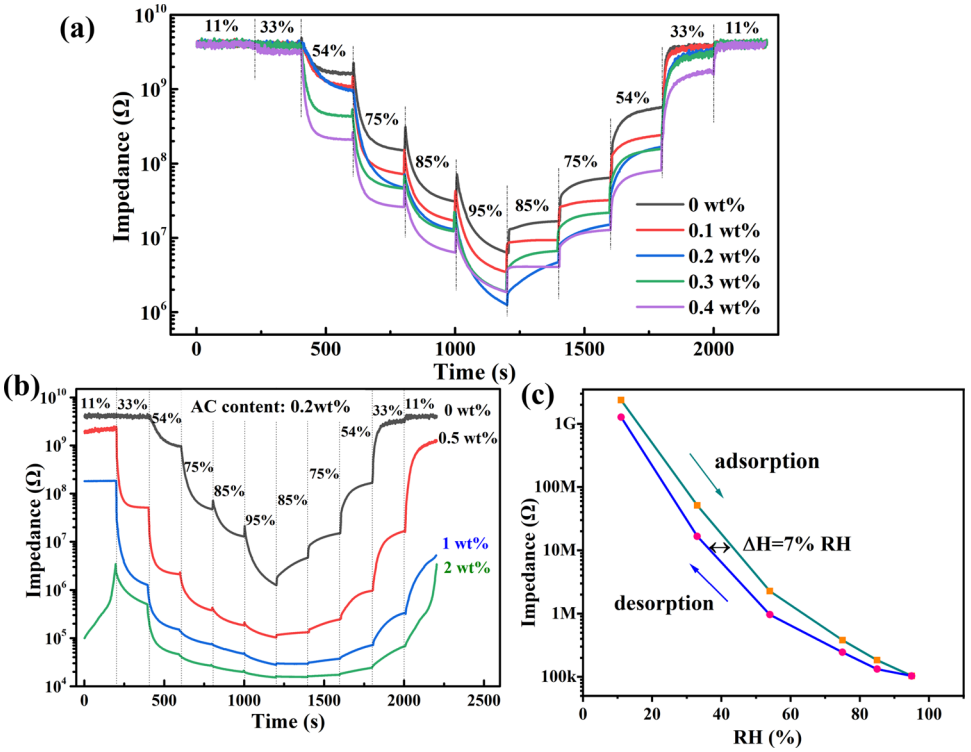

Figure 4. (a) Impedance variation curves of the sensors with different AC mass fractions under different RH levels. (b) Impedance variation curves of humidity sensors with different $MgCl_2{\cdot}6H_2O$ mass fractions (AC content of 0.2 wt %) under different RHs. (c) Humidity hysteresis characteristic of the BC/AC/$MgCl_2$ based humidity sensor (AC content of 0.2 wt %, $MgCl_2{\cdot}6H_2O$ content of 0.5 wt %).

there are C, Mg, and Cl elements on the film surface. Mg, Cl, and O elements originating from the hydrophilic material $MgCl_2{\cdot}6H_2O$ are all distributed uniformly on the film surface. Some of the O elements originate from the BC. The elemental mapping image of C shows a uniform distribution from the BC, while the stronger C signals are from active carbon (see the SEM image for elemental mapping in Figure S3). XRD patterns of the BC, BC/AC/$MgCl_2$ film, and the AC, $MgCl_2$ powers were collected to confirm the crystalline information on them (Figure 3b). The BC and BC/AC/$MgCl_2$ displayed similar peaks at 2θ angles of about 14.3° and 22°, which correspond to the (1−10, 200) planes of typical cellulose I.[34]

https://doi.org/10.1021/acsomega.4c05316
ACS Omega 2024, 9, 33261−33269

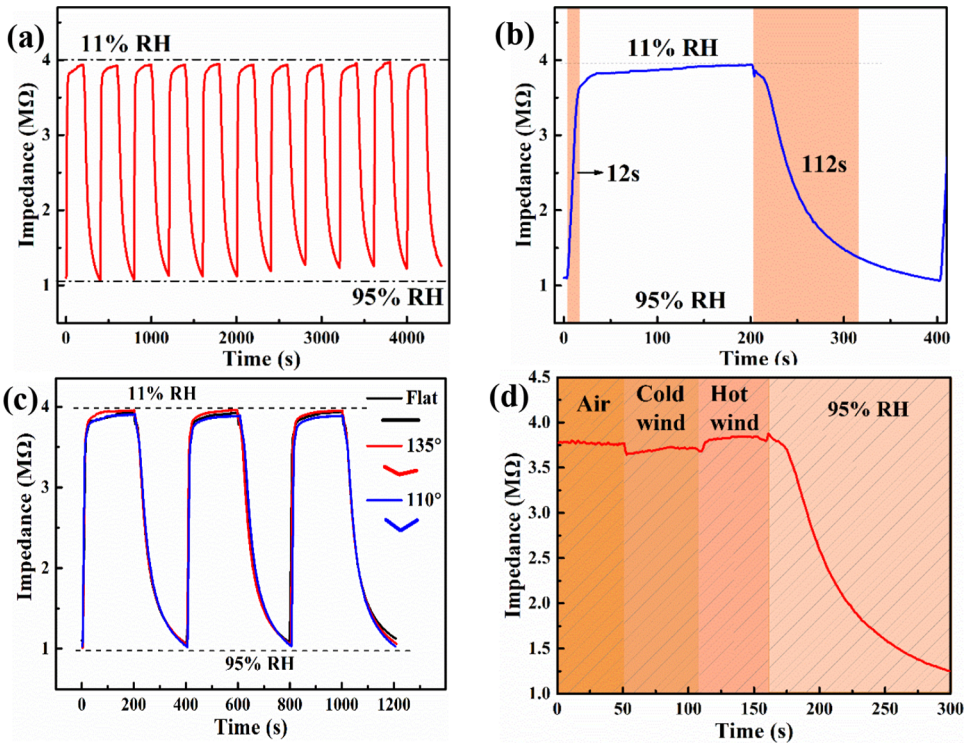

Figure 5. (a) Impedance variation curves of the humidity sensor with RH from 11 to 95% for 11 successive cycles. (b) Response and recovery time of the sensor from RH 11−95%. (c) Impedance variation curves in different bending states. (d) Impedance variation curve in a hair dryer experiment.

Various types of cellulose have been reported for the fabrication of the humidity sensor as well as other gas sensors.[19,23,26−29,35−37] Besides, the BC solution was applied in this work because of the suitable fluidity and good film formation performance, which is an important factor to consider in printing technology. There is no diffraction peak for AC, indicating the amorphous nature of the active carbon. Besides, the typical peaks of crystallized $MgCl_2$ were not observed in the BC/AC/$MgCl_2$, indicating that the loaded $MgCl_2$ exhibited an amorphous state in the composite film.

The sensitive properties of the humidity sensor are closely related to the water adsorption capacity of the sensitive layer. Hence, the hydrophilic surface is the basic requirement for the humidity sensing material, and the hydrophilicity of the sensing layer plays a crucial role in the sensing performance. The contact angle of the BC/AC/$MgCl_2$ sensing film was measured to evaluate the hydrophobic and hydrophilic performance. It is worth noting that a printed planar film with the same composition (0.2 wt % AC and 0.5 wt % $MgCl_2$) was employed in the test instead of the mesh film for full contact with the water droplet. In the experiment, the dynamic changes in contact angle were recorded for both the pure BC film and the BC/AC/$MgCl_2$ sensing film. As shown in Figure 3c,d, when a water droplet initially contacted the surface of the pure BC film, the contact angle was close to 90°. It decreased to 74.7° within 5 s and further decreased to 55.4° within 100 s (Figure 3c1,c2). On the other hand, the hydrophilic property of the BC/AC/$MgCl_2$ composite film was measured in the same way. As illustrated in Figure 3d1,d2, the contact angle underwent a noticeable decrease to 31.3° within 0.2 s. By 0.7 s, the water droplet lay flat on the composite film surface so that the instrument could hardly capture the contact angle data. The significantly improved hydrophilicity was caused by the addition of the hygroscopic $MgCl_2$ that enhanced the water absorption capacity of the sensing film. It can capture water molecules from the environment rapidly and spread into the film to improve the humidity-sensitive characteristics of the sensing layer. Although the hydrophilic groups and porous surface (Figure 2a) of the BC film endow it with hydrophilicity to some extent, the addition of $MgCl_2$ enhanced the water absorption ability and hydrophilicity significantly.

Optimization of Sensitive Film Composition. As an advanced manufacturing technology, 3D printing has been applied to the fabrication of various sensors. Some of the research used a 3D printing process to make the electrodes of the sensor,[26] while some others to the fabrication of a sensitive layer.[22] It has the advantage of more freedom in film pattern and thickness design as compared to the coating method. An additional basic requirement for the sensing material is the formation of a continuous and stable print jet by the specific printing technology, which needs optimization of the sensitive material composition.

Figure 4a shows the impedance response curves of flexible BC/AC humidity sensors prepared with AC mass fractions of 0, 0.1, 0.2, 0.3, and 0.4 wt %. The lowest RH achieved was 11% due to experimental restriction. All of the prepared sensors can respond to RH change in the form of corresponding impedance variations. The impedance of all the humidity sensors decreased when the RH increased gradually from 11 to 95%, and then increased stepwise when the RH decreased to 11%. It is seen that the pure BC film without AC responds to RH change, indicating the hydrophilic property of the BC substrate. Because of the rich hydroxyl and carboxyl functional groups on its surface, BC can be positively or negatively charged by water absorption. The addition of AC improved the conductivity of the film, especially in a humid environment. As

https://doi.org/10.1021/acsomega.4c05316
ACS Omega 2024, 9, 33261−33269

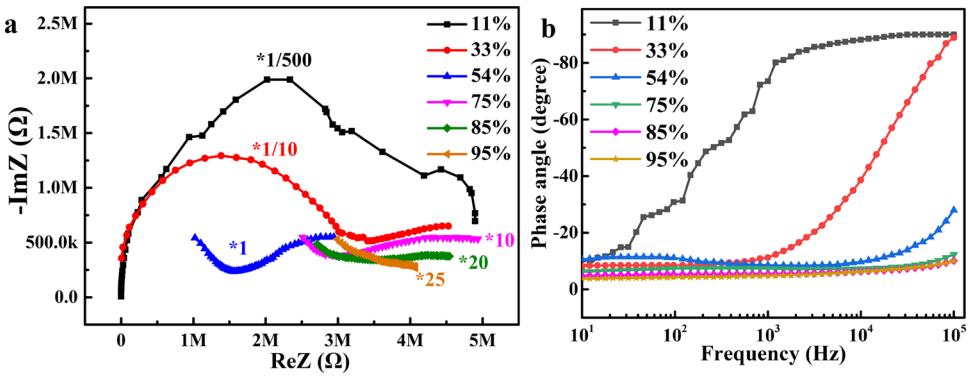

Figure 6. (a) Complex impedance spectra of the sensor under different RHs. (b) Frequency-phase angle spectra of the sensor under different RHs and frequencies.

the mass fraction of AC increased, a higher impedance response was observed for the same humidity change, especially at a low humidity range from 11 to 33%. However, much more AC added (exceeds 0.2 wt %) decreased the response of the sensor at high RH from 85 to 95%. The dispersed AC in the sensing film acted as a conductive filler by electronic conducting. The expansion of the BC induced by water absorption changed the distance of AC particles to decrease the conductivity of the AC part. However, the ionic conductivity was enhanced because of the water absorption. As a result, the BC/AC composite film with an AC mass fraction of 0.2 wt % was selected for further optimization. Figure 4b illustrates the impedance response curves of the BC/AC/$MgCl_2$-based flexible humidity sensors with $MgCl_2{\cdot}6H_2O$ mass fractions of 0.5, 1, and 2 wt % under different RHs. It is obvious that the addition of $MgCl_2{\cdot}6H_2O$ enhanced the sensor response, especially for a low RH range from 11 to 33%. However, the excess mass fraction of $MgCl_2{\cdot}6H_2O$ than 0.5 wt % showed a negative impact on the recovery speed of the sensor. When the mass fraction of $MgCl_2{\cdot}6H_2O$ reached 2 wt %, the BC/AC/$MgCl_2$ sensing film was hygroscopic enough to absorb moisture from the environment within RH of 54%. The impedance response to the RH change was weak when further increasing RH from 54 to 95% because of absorption saturation. Therefore, BC/AC/$MgCl_2$ sensing film with AC content of 0.2 wt % and $MgCl_2{\cdot}6H_2O$ content of 0.5 wt % was chosen for the subsequent investigations and applications. Figure 4c depicts the mild hysteresis of 7% RH in the absorption and desorption processes of the printed humidity sensor.

The repeatability and long-term stability of humidity sensors are also crucial properties for practical applications. After storing for about 1 month, the sensor was tested for its repeatability to humidity as shown in Figure 5a. The impedance of the sensor increased rapidly when moving from an RH of 11−95%, and decreased to an initial impedance value when moving back to an RH of 11%. The response was stable in the 11 consecutive cycles, indicating the satisfying stability as well as good long-term stability of the prepared humidity sensor. The response and recovery time (defined as the time span to reach 90% of the total impedance change) of the humidity sensor was calculated accordingly. As the impedance variation curve shown in Figure 5b, the response time was calculated to be 12 s and the recovery time 112 s. Although the recovery is somewhat slurry because of the strong hydrophilicity of the sensing film. It would not affect the practical application of the sensor, where the change in impedance is enough without full recovery. The sensor was also tested for its flexibility by recording the response to humidity in three different bending states, i.e., 180°, 135°, and 110° (see the digital photo in Figure S4). As shown in Figure 5c, the impedance variation curves were almost overlapped in the three bending angles, indicating the satisfying flexibility of the printed sensor. A simple hair dryer experiment was implemented to investigate the effect of the temperature on the humidity sensor response. Specifically, the sensor was put in air conditioning, blown by cold air and hot air, and then moved to RH of 95% condition. As shown in Figure 5d, there is a slight decrease in impedance when blown by cold air, while there is a slight increase when blown by hot air as compared to that in air condition. The impedance decreased drastically when moving to RH or 95%. This simple experiment demonstrates that temperature has little effect on the impedance of the humidity sensor.

Sensing Mechanism Exploration. To investigate the fundamental sensing principle of the BC/AC/$MgCl_2$-based humidity sensor, complex impedance spectra were collected at different RHs and frequencies. As shown in Figure 6a, the complex impedance curve of the sensitive layer approached a semicircle under RH of 11%. Ionization rarely occurred because the vapor was little at this low RH. As a result, the conductivity was mainly attributed to the electron transition by AC in the film. At a higher RH of 33%, the complex impedance plots consist of two parts: a semicircle at high frequency and a straight line at low frequency. Water molecules absorbed by the BC/AC/$MgCl_2$ sensor would dissolve into H^+ and OH^- ions (eq 1), which can travel in the film through the proton exchange mechanism.[38,39] Besides, Mg^{2+} and Cl^- generated by $MgCl_2$ (eq 2) can also move freely to produce ionic conduction. When H^+, Mg^{2+}, and Cl^- ions take part in conduction, the straight line will be observed on the complex impedance plots. The semicircle becomes flattened and the straight line becomes more obvious when the RH is further increased to higher than 54%, indicating that ionic conduction plays a major role. When the humidity reaches 95%, the semicircular shape disappears indicating that the electronic conduction is negligible. One can conclude that there is saturation for the humidity response because there are limited ions in the BC/AC/$MgCl_2$ film.

$$H_2O \rightarrow H^+ + OH^- \quad (1)$$

$$MgCl_2 \rightarrow Mg^{2+} + 2Cl^- \quad (2)$$

https://doi.org/10.1021/acsomega.4c05316
ACS Omega 2024, 9, 33261−33269

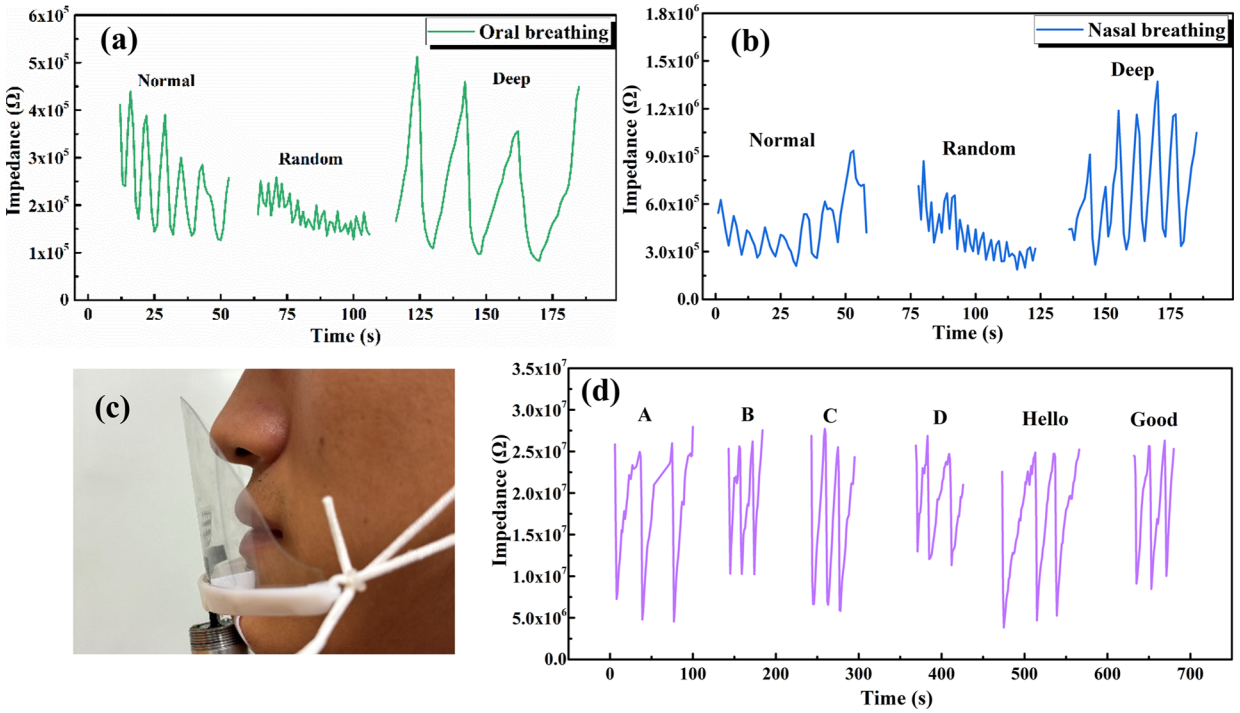

Figure 7. Impedance-time curves of simulated human oral breathing (a) and nasal breathing (b) at different frequencies. (c) Digital photo of the volunteer wearing masking on which the BC/AC/$MgCl_2$ sensor was fixed. (d) Repeated response to the speaking of different words.

Figure 6b depicts the variation of phase angle with frequency for the BC/AC/$MgCl_2$ sensor at different RHs. At an RH of 11%, the phase angle decreased from −12° to −90° as the frequency increased, indicating that the BC/AC/$MgCl_2$ sensor tends to be a resistive device at low frequency and a capacitive device at high frequency. At the operating frequency of 100 Hz, the sensor exhibited resistive character at RH higher than 11% because of the ionic conductivity.

APPLICATION TESTING OF HUMIDITY SENSOR

Monitoring of Human Respiration. To demonstrate the application of the developed humidity sensor in human respiration monitoring, it was attached to a mask and placed approximately 3 cm away from the volunteer's mouth and nose. Normal, rapid, and deep breathing was performed through the mouth and nose to simulate respiratory frequencies under different exercise conditions. As shown in Figure 7a, when the volunteer breathed normally through their nose, the humidity around the sensor increased during exhalation, resulting in a decrease in the impedance. Conversely, impedance increased rapidly during inhalation. After several cycles of breathing, the overall impedance of the sensor exhibited an upward trend. The impedance response for the nasal breathing test shows a similar result, as listed in Figure 7b. Breathing behaviors including frequency of normal, rapid, and deep breathing through the nose and mouth were calculated to be 5, 3, and 10 s/breath, corresponding to 12 bpm (breaths/min), 20 bpm, and 6 bpm. The slower the exhalation rate, the longer the duration of each exhalation, leading to a higher surface humidity and a greater change in impedance. Conversely, a faster exhalation rate results in lower humidity and impedance changes. The response and recovery speed of the prepared humidity sensor can be further improved, which is enough for respiratory monitoring applications.

Speech Monitoring and Recognition. The sensor was placed approximately 3 cm away from a volunteer's mouth to verify the feasibility of the prepared humidity sensor for speech recognition (Figure 7c). When the volunteer pronounced six words of "a," "b," "c," "d," "hello," and "good" to simulate daily conversations, the amount of moisture exhaled from the mouth varied with different pronunciations. As shown in Figure 7d, the exhalation of "a," "c," and "hello" contained significantly more moisture than the other three words, resulting in a larger variation in the impedance of the sensor. By comparing "a" with "c" and "b" with "d", one can observe that the duration of the pronunciation of "a" and "d" was longer than the other two. Consequently, the time taken for the impedance change, or the response and recovery time of the sensor, was also longer for these sounds. Based on these observations, it can be concluded that the sensor can distinguish between simulated speech sounds by analyzing both the numerical humidity response and the duration from response to recovery. Therefore, the sensor fulfills the function of speech monitoring.

Noncontact Switch Test. Humidity sensor-based noncontact switches can be used in human−machine interactions or wireless locations. Since the humidity of human skin is generally higher than the ambient humidity, it can be used as a stimulus for a humidity sensor. As inserted in Figure 8, a finger was placed a certain height above the surface of the sensor for 5 s, and then removed for another 5 s to verify the noncontact sensing. As seen, the impedance change relies on the finger distance, the closer the distance, the lower the impedance. The sensor is able to respond promptly to the approach and departure of the finger, indicating its application potential in noncontact switching and object positioning.

CONCLUSIONS

In summary, a meshed, self-supporting, and flexible humidity sensor was fabricated by a simple printing method on a

https://doi.org/10.1021/acsomega.4c05316
ACS Omega 2024, 9, 33261−33269

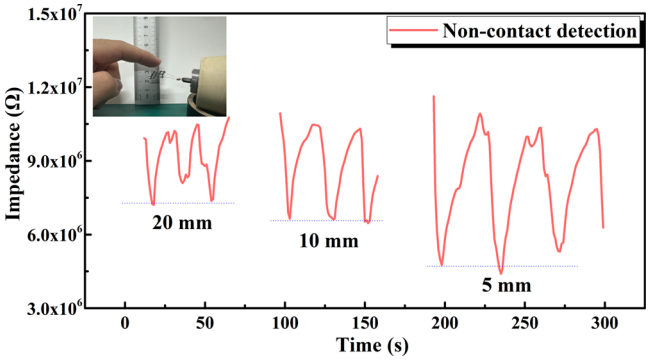

Figure 8. Impedance variation curves of the noncontact experiment.

homemade two-dimensional stepping numerical control workstation. The sensitive layer, flexible substrate, and electrodes were integrated into one of the BC/AC/$MgCl_2$ self-supporting sensors. The preparation process was simplified, and the structure of the sensor was integrated. Experimental results demonstrate that the sensor exhibits a highly sensitive response to a wide RH range of 11−95% with validated stability and reliability. Complex impedance spectra results demonstrated that the ionic conduction played the dominant role in the sensor response in RH higher than 11%. The prepared humidity sensor showed satisfying sensing properties that can be applied for human respiration monitoring, speech recognition, and noncontact locating. The abundant, cost-effective, and eco-friendly BC and AC combined with the facile preparation technique in this work could provide a useful strategy for developing a multifunctional humidity sensor.

■ ASSOCIATED CONTENT

Supporting Information

The Supporting Information is available free of charge at https://pubs.acs.org/doi/10.1021/acsomega.4c05316.

SEM images of pure bacterial cellulose, composite film with 0.2 wt % AC, composite film with 0.4 wt % AC, composite film with 0.2 wt % AC and 0.5 wt % $MgCl_2$, composite film with 0.2 wt % AC and 1 wt % $MgCl_2$; SEM image of the composite film with 0.2 wt % AC and 1 wt % $MgCl_2$; SEM image for the elemental mapping (0.2 wt % AC and 0.5 wt % $MgCl_2$); and digital photo of the sensor bent for the flexible experiment (PDF)

■ AUTHOR INFORMATION

Corresponding Author

Chengli Tang − *School of Mechanical Engineering, Tianjin University, Tianjin 300354, China; Zhejiang Zhongda Advanced Material Co., Ltd., Jiaxing 314312, China; College of Information Science and Engineering, Jiaxing University, Jiaxing 314001, China;* orcid.org/0000-0002-8361-3878; Email: tcl-lily@zjxu.edu.cn

Authors

Haoxiang Wang − *College of Information Science and Engineering, Jiaxing University, Jiaxing 314001, China; School of Mechanical Engineering, Zhejiang Sci-Tech University, Hangzhou 310018, China*

Yuhao Dou − *College of Information Science and Engineering, Jiaxing University, Jiaxing 314001, China; School of Mechanical Engineering, Zhejiang Sci-Tech University, Hangzhou 310018, China*

Puguo Lai − *College of Information Science and Engineering, Jiaxing University, Jiaxing 314001, China*

Complete contact information is available at: https://pubs.acs.org/10.1021/acsomega.4c05316

Notes

The authors declare no competing financial interest.

■ ACKNOWLEDGMENTS

This work was supported by the National Natural Science Foundation of China (grant number 61704067); the Top-level Talent Project of Zhejiang Province; the Public Welfare Project of Jiaxing Science and Technology Bureau (grant number 2021AY10066); and the Key Project of Student Research Training of Jiaxing University (8517231259).

■ REFERENCES

(1) Ma, L.; Wu, R.; Patil, A.; Zhu, S.; Meng, Z.; Meng, H.; Hou, C.; Zhang, Y.; Liu, Q.; Yu, R.; Wang, J.; Lin, N.; Liu, X. Full-Textile Wireless Flexible Humidity Sensor for Human Physiological Monitoring. *Adv. Funct. Mater.* **2019**, *29* (43), No. 1904549.

(2) Zhang, X.; He, D.; Yang, Q.; Atashbar, M. Rapid, Highly Sensitive, and Highly Repeatable Printed Porous Paper Humidity Sensor. *Chem. Eng. J.* **2022**, *433*, No. 133751.

(3) Duan, Z.; Jiang, Y.; Tai, H. Recent Advances in Humidity Sensors for Human Body Related Humidity Detection. *J. Mater. Chem. C* **2021**, *9* (42), 14963−149680.

(4) Li, C.; Liu, J.; Peng, H.; Sui, Y.; Song, J.; Liu, Y.; Huang, W.; Chen, X.; Shen, J.; Ling, Y.; Huang, C.; Hong, C.; Hong, Y.; Huang, W. A Camel Nose-Inspired Highly Durable Neuromorphic Humidity Sensor with Water Source Locating Capability. *ACS Nano* **2022**, *16* (1), 1511−1522.

(5) Xu, L.; Zhai, H.; Chen, X.; Liu, Y.; Wang, M.; Liu, Z.; Umar, M.; Ji, C.; Chen, Z.; Jin, L.; Li, Y.; Ye, T. Coolmax/graphene-oxide Functionalized Textile Humidity Densor with Ultrafast Response for Human Activities Monitoring. *Chem. Eng. J.* **2021**, *412*, No. 128639.

(6) Duan, Z.; Jiang, Y.; Zhao, Q.; Huang, Q.; Wang, S.; Zhang, Y.; Wu, Y.; Liu, B.; Zhen, Y.; Tai, H. Daily Writing Carbon Ink: Novel Application on Humidity Sensor with Wide Detection Range, Low Detection Limit and High Detection Resolution. *Sensor Actuat B-Chem.* **2021**, *339*, No. 129884.

(7) Li, N.; Jiang, Y.; Zhou, C.; Xiao, Y.; Meng, Bo; Wang, Z.; Huang, D.; Xing, C.; Peng, Z. High-Performance Humidity Sensor Based on Urchin-Like Composite of Ti3C2MXene-Derived TiO2 Nanowires. *ACS Appl. Mater. Interfaces* **2019**, *11* (41), 38116−38125.

(8) Duan, Z.; Zhao, Q.; Wang, S.; Yuan, Z.; Zhang, Y.; Li, X.; Wu, Y.; Jiang, Y.; Tai, H. Novel Application of Attapulgite on High Performance and Low-cost Humidity Sensors. *Sensor Actuat B- Chem.* **2020**, *305*, No. 127534.

(9) Dinh, T.; Phan, H.; Nguyen, T.; Qamar, A.; Foisal, A.; Viet, T.; Tran, C.; Zhu, Y.; Nguyen, N.; Dao, D. Environment-friendly Carbon Nanotube Based Flexible Electronics for Noninvasive and Wearable Healthcare. *J. Mater. Chem. C* **2016**, *4* (42), 10061−10068.

(10) Kanaparthi, S. Pencil-drawn Paper-based Non-invasive and Wearable Capacitive Respiration Sensor. *Electroanal* **2017**, *29* (12), 2680−2684.

(11) Balakrishnan, V.; Dinh, T.; Foisal, A.; Nguyen, T.; Phan, H.; Dao, D.; Nguyen, N. Paper-Based Electronics Using Graphite and Silver Nanoparticles for Respiration Monitoring. *IEEE Sens J.* **2019**, *19* (24), 11784−11790.

(12) Gîder, F.; Ainla, A.; Redston, J.; Mosadegh, B.; Glavan, A.; Martin, T.; Whitesides, G. Paper-Based Electrical Respiration Sensor. *Angew. Chem., Int. Ed.* **2016**, *55*, 5727−5732.

(13) Li, S.; Zhang, Y.; Wang, Y.; Xia, K.; Yin, Z.; Wang, H.; Zhang, M.; Liang, X.; Lu, H.; Zhu, M.; Wang, H.; Shen, X.; Zhang, Y. Physical Sensors for Skin-inspired Electronics. *Infomat* **2020**, *2* (1), 184−211.

(14) Vincenzo, C.; Giacomo, T.; Milan, P.; Mario, M.; Beatriz, M.; Susana, G.; Mehdi, K.; Anders, K.; Athanassia, A.; Roberto, C.; Volker, J.; Marco, S.; Francesco, B.; Roman, K.; José, A. Biodegradable and Insoluble Cellulose Photonic Crystals and Metasurfaces. *ACS Nano* **2020**, *14* (8), 9502−9511.
(15) Benjamin, J.; Lewis, K. Sleep-disordered breathing and cardiovascular risk. *Postgrad. Med. J.* **2008**, *84*, 15−22.
(16) Li, S.; Zhang, Y.; Liang, X. P.; Wang, H. M.; Lu, H. J.; Zhu, M. J.; Wang, H. M.; Zhang, M. C.; Qiu, X. P.; Song, Y. F.; Zhang, Y. Y. Humidity-sensitive Chemoelectric Flexible Sensors based on Metal-air Redox Reaction for Health Management. *Nat. Commun.* **2022**, *13*, 5416.
(17) Wu, J.; Sun, Y. M.; Wu, Z. X.; Li, X.; Wang, N.; Tao, K.; Wang, G. P. Carbon Nanocoil-Based Fast-Response and Flexible Humidity Sensor for Multifunctional Applications. *ACS Appl. Mater. Interfaces* **2019**, *11* (4), 4242−4251.
(18) Pereira, N. M.; Rezende, N. P.; Cunha, T. H. R.; Barboza, A. P. M.; Silva, G. G.; Lippross, D.; Neves, B. R. A.; Chacham, H.; Ferlauto, A. S.; Lacerda, R. G. Aerosol-Printed MoS_2 Ink as a High Sensitivity Humidity Sensor. *ACS Omega* **2022**, *7* (11), 9388−9396.
(19) Zhu, P. H.; Qu, H. J.; Kuang, Y. D.; Hao, L. J.; Diao, J. J.; Chen, G. Cellulose Nanofiber/Carbon Nanotube Dual Network-Enabled Humidity Sensor with High Sensitivity and Durability. *ACS Appl. Mater. Interfaces* **2020**, *12* (29), 33229−33238.
(20) Li, S.; Wan, T.; Wei, H. G.; Wang, S. Y.; Wang, B.; Cheng, B. W. Flexible Highly-Sensitive Humidity Sensor based on CGO/SMPLAF for Wearable Human Skin Humidity Detection. *Sensor Actuat B- Chem.* **2022**, *362*, No. 131806.
(21) Guan, X.; Yu, Y. L.; Hou, Z. M.; Wu, K.; Zhao, H. R.; Liu, S.; Fei, T.; Zhang, T. A flexible humidity sensor based on self-supported polymer film. *Sensor Actuat B- Chem.* **2022**, *358*, No. 131438.
(22) Pan, T.; Yu, Z.; Huang, F.; Yao, H.; Hu, G.; Tang, C.; Gu, J. Flexible Humidity Sensor with High Sensitivity and Durability for Respiratory Monitoring Using Near-Field Electrohydrodynamic Direct-Writing Method. *ACS Appl. Mater. Interfaces* **2023**, *15* (23), 28248−28257.
(23) Wang, H. X.; Tang, C. L.; Xu, J. A Highly Sensitive Flexible Humidity Sensor based on Conductive Tape and a Carboxymethyl Cellulose@graphene Composite. *RSC Adv.* **2023**, *13*, 27746.
(24) Wang, Y.; Zhou, Y.; Xie, G.; Li, J.; Wang, Y.; Liu, X.; Zang, Z. Dual Resistance and Impedance Investigation: Ultrasensitive and Stable Humidity Detection of Molybdenum Disulfide Nanosheet Polyethylene Oxide Hybrids. *ACS Appl. Mater. Interfaces* **2021**, *13*, 25250−25259.
(25) Li, J.; Zhou, Y.; Wang, Y.; Zhou, S.; Zhang, R.; Wang, Y.; Zang, Z. Improving Humidity Sensing of Black Phosphorus Nanosheets by Co-Doping Benzyl Viologen and Au Nanoparticles. *J. Electrochem. Soc.* **2022**, *169*, No. 017513.
(26) Zhu, P. H.; Liu, Y.; Fang, Z. Q.; Kuang, Y. D.; Zhang, Y. Z.; Peng, C. X.; Chen, G. Flexible and Highly Sensitive Humidity Sensor Based on Cellulose Nanofibers and Carbon Nanotube Composite Film. *Langmuir* **2019**, *35* (14), 4834−4842.
(27) Wang, Y.; Zhang, L. N.; Zhou, J. P.; Lu, A. Flexible and Transparent Cellulose-Based Ionic Film as a Humidity Sensor. *ACS Appl. Mater. Interfaces* **2020**, *12* (6), 7631−7638.
(28) Guan, X.; Hou, Z. N.; Wu, K.; Zhao, H. R.; Liu, S.; Fei, T.; Zhang, T. Flexible humidity sensor based on modified cellulose paper. *Sensor Actuat B- Chem.* **2021**, *339*, No. 129879.
(29) Zhu, L. T.; Li, X.; Kasuga, T.; Uetani, K.; Nogi, M.; Koga, H. All-cellulose-derived humidity sensor prepared via direct laser writing of conductive and moisture-stable electrodes on TEMPO-oxidized cellulose paper. *J. Mater. Chem. C* **2022**, *10*, 3712.
(30) Kim, J.; Kim, S.; Kil, H.; Kim, Y.; Park, J. Highly Conformable, Transparent Electrodes for Epidermal Electronics. *Nano Lett.* **2018**, *18* (7), 4531−4540.
(31) Ha, T.; Tran, J.; Liu, S.; Jang, H.; Jeong, H.; Mitbander, R.; Huh, H.; Qiu, Y.; Duong, J.; Wang, R.; Wang, P.; Tandon, A.; Sirohi, J.; Lu, N. A Chest-Laminated Ultrathin and Stretchable E-Tattoo for the Measurement of Electrocardiogram, Seismocardiogram, and Cardiac Time Intervals. *Adv. Sci.* **2019**, *6*, No. 1900290.
(32) Pan, S.; Zhang, F.; Cai, P.; Cai, P.; Wang, M.; He, K.; Luo, Y.; Li, Z.; Chen, G.; Ji, S.; Liu, Z.; Loh, X.; Chen, X. Mechanically Interlocked Hydrogel−Elastomer Hybrids for On-Skin Electronics. *Adv. Funct. Mater.* **2020**, *30* (29), No. 1909540.
(33) Ryotaro, M.; Akihito, M.; Tomoyuki, Y.; Takao, S. Skin Impedance Measurements with Nanomesh Electrodes for Monitoring Skin Hydration. *Adv. Healthcare Mater.* **2020**, *9*, No. 2001322.
(34) Kuang, Y.; Chen, G.; Ming, S.; Wu, Z.; Fang, Z. Solvent Resistance of 2,2,6,6-Tetramethylpiperidine-1-oxyl (TEMPO) Treated Cellulose Nanofiber Film for Flexible Electronics. *Cellulose* **2016**, *23*, 1979−1987.
(35) Li, J.; Zhao, H.; Wang, Y.; Zhang, R.; Zou, C.; Zhou, Y. Mesoporous WS2-Decorated Cellulose Nanofiber-Templated CuO Heterostructures for High-Performance Chemiresistive Hydrogen Sulfide Sensors. *Anal. Chem.* **2022**, *94*, 16160−16170.
(36) Zhang, R.; Wang, Y.; Li, J.; Zhao, H.; Wang, Y.; Zhou, Y. Mesoporous Cellulose Nanofibers-interlaced PEDOT:PSS Hybrids for Chemiresistive Ammonia Detection. *Microchim. Acta* **2022**, *189*, No. 308.
(37) Zhou, Y.; Zhang, R.; She, X.; Li, J.; Zhao, H.; Wang, Y.; Chen, Y.; Xie, L.; Zou, C.; Li, X. Alkalized Cellulose Nanofiber-Interweaved PEDOT:PSS Thin-Film Sensors via Layer-by-Layer Spraying Assembly for Ultrafast Molecular Ammonia Detection. *ACS Appl. Mater. Interfaces* **2023**, *15*, 53802−53814.
(38) Gupta, A.; Sakhuja, N.; Jha, R.; Bhat, N. Ultrasensitive Chemiresistive Humidity Sensor Based on Gold Functionalized WS_2 nanosheets. *Sensor Actuat A-Phys.* **2021**, *331*, No. 113008.
(39) Na, B.; Guo, C.; Wang, T.; Zhang, X.; Huo, L.; Li, L.; Liu, Y.; Cheng, X.; Xu, Y. Multifunctional and Highly Sensitive Humidity Sensor Based on KCl/Sm_2O_3 Nanoflowers with Ultrafast Response. *Sensor Actuat B- Chem.* **2023**, *385*, No. 133701.

https://doi.org/10.1021/acsomega.4c05316
ACS Omega 2024, 9, 33261−33269